Noise-driven velocity selection in persistent reaction random walks: Renormalization theory and numerical validation

D. C. Bitang Á Ziem *

Department of Electrical and Telecommunications Engineering, National Advanced School of Engineering of Yaounde, P. O. Box 8390, Yaounde, Cameroon

and Department of Electrical Engineering, École Supérieure des Techniques Avancées pour le Développement (ESTAD), P.O. Box 14601, Yaounde, Cameroon

(Received 1 April 2026; revised 29 August 2026; accepted 22 October 2026; published 4 November 2026)

Front propagation in nonlinear systems is a central theme across physics and biology, yet classical diffusion-based models fail to capture finite-speed transport and directional persistence. In this work, we investigate the impact of multiplicative noise on persistent reaction random walks, focusing on velocity selection in both pushed and pulled regimes. Using nonperturbative renormalization theory, we derive effective reaction terms that reveal how fluctuations reshape the balance between growth and mortality. We predict a systematic stochastic acceleration alongside a qualitative inversion of noise effects depending on the stability parameter a: in strongly pushed fronts ($a \geqslant 0.7$), noise reduces the recession speed by lowering the Allee threshold via a renormalized effective parameter $a_{\text{eff}} = a - s/2$. In the pulled regime ($a < 0$), an unconditional acceleration is observed, driven by a linear noise-induced growth term at the leading edge. These analytical predictions are validated by high-resolution stochastic simulations ($M = 100$) utilizing a Split-Heun scheme to strictly enforce the Stratonovich interpretation. The numerical results show clear quantitative agreement with the theory, confirming the strong predictive power of our effective framework. Crucially, because the noise corrections are strictly reactive, they remain completely decoupled from the hyperbolic transport mechanism—a structural feature that allows the noise signature to robustly persist across the hyperbolic-to-diffusive transport transition.

DOI: 10.1103/ngqz-qtzj

I. INTRODUCTION

Front propagation in spatially extended systems remains a cornerstone of nonlinear science, shaping phenomena from ecological invasions [1,2] and chemical pattern formation [3] to neural signaling [4] and engineered transport processes [5]. Classical paradigms such as the Nagumo equation [6] and the Fisher-Kolmogorov-Petrovsky-Piskunov (FKPP) framework [7] have provided enduring insights into traveling waves in diffusive media. Yet these models assume infinitesimal steps and neglect directional persistence, an assumption increasingly challenged by modern applications involving cellular migration or active matter.

Persistent random walks offer a more realistic description of transport in regimes where agents move with finite speed and correlated trajectories [8–15]. In this context, the direction-independent random walk (DIRW) transport sector shares deep theoretical foundations with the continuum descriptions of run-and-tumble particles and persistent self-propelled active matter [16–18]. Exploring how localized reaction kinetics interact with directional persistence has thus become crucial. To capture these features, we replace diffusion by a direction-independent reaction walk (DIRW) system [14]:

$$\frac{\partial u^+}{\partial t} + \gamma \frac{\partial u^+}{\partial r} = \mu(u^- - u^+) + \frac{1}{2}b(u) - d(u)u^+, \tag{1}$$

$$\frac{\partial u^-}{\partial t} - \gamma \frac{\partial u^-}{\partial r} = \mu(u^+ - u^-) + \frac{1}{2}b(u) - d(u)u^-, \tag{2}$$

where $u = u^+ + u^-$ is the total density, γ is the particle speed, and μ the turning frequency. To connect this hyperbolic transport model to the bistable and unstable kinetics of the Nagumo equation, the birth and death terms are explicitly constructed to inherit the stability properties dictated by the control parameter a. In the pushed regime ($a > 0$), they take the form

$$b(u) = (1 + a)u^2, \quad d(u) = u^2 + a \quad (a > 0), \tag{3}$$

while in the pulled regime ($a < 0$), they take the form

$$b(u) = (1 + a)u^2 - au, \quad d(u) = u^2 \quad (a < 0). \tag{4}$$

For $a > 0$, the state $u = 0$ is metastable and fronts are pushed; for $a < 0$, it is unstable and fronts are pulled [19].

Noise has long been recognized as a key modifier of front dynamics. While additive noise typically broadens velocity distributions without altering the mean [20], multiplicative noise can fundamentally reshape propagation by renormalizing reaction terms [21,22]. Nonperturbative renormalization techniques, employing the Furutsu-Novikov-Donsker theorem [23–25], decouple noise statistics from mean-field

*Contact author: daniel.bitang@univ-yaounde1.cm

Published by the American Physical Society under the terms of the Creative Commons Attribution 4.0 International license. Further distribution of this work must maintain attribution to the author(s) and the published article's title, journal citation, and DOI.

dynamics. In this study, we apply this framework to the DIRW system. In Sec. II, we derive the exact effective reaction kinetics and present analytical predictions for velocity selection under noisy environments. In Sec. III, we subject these predictions to high-resolution stochastic simulations, demonstrating how the Stratonovich-induced linear growth enhancement and effective mortality reduction dictate the macroscopic velocity selection, confirming the strong quantitative agreement of our effective framework.

II. NONLINEAR ANALYSIS: PREDICTIONS FROM RENORMALIZED FIELD-MEAN DYNAMICS

Before proceeding to numerical integration, we can extract valuable physical insights by directly inspecting the algebraic structure of the renormalized reaction terms derived via the Furutsu-Novikov-Donsker framework in Appendix B. Replacing the deterministic birth and death functions with their effective counterparts, $b^{\mathrm{ren}}(U)$ and $d^{\mathrm{ren}}(U)$, reveals how the single noise parameter s reshapes the macrotransport balance between growth and mortality.

Briefly, the FND procedure maps the stochastic multiplicative term $\langle g_1(u^+, u^-)\xi(t)\rangle$ onto a deterministic correction ΔR^+ by evaluating the functional derivative of the reaction sensitivity with respect to the noise history. Operating under the physically motivated Stratonovich interpretation (representing the white-noise limit of a short-correlated environmental process), this closure yields a nonzero noise-induced drift. The resulting effective reaction terms, $b_{\mathrm{ren}}(U)$ and $d_{\mathrm{ren}}(U)$, incorporate algebraic corrections proportional to the noise intensity s, which systematically reshape the growth and mortality balance without altering the underlying hyperbolic transport operator. The rigorous step-by-step derivation of these terms is provided in Appendix B. In this section, we translate these mathematical modifications into testable predictions regarding the asymptotic front velocity, establishing a rigorous framework that completely bypasses external phenomenological assumptions.

A. Pushed regime ($a > 0$)

The effective kinetics governing the pushed regime are given by $b^{\mathrm{ren}}_{\mathrm{psd}}(U) = sU^3 + (1 + a - 1.5s)U^2$ and $d^{\mathrm{ren}}_{\mathrm{psd}}(U) = U^2 + a - 0.5s$. A close examination reveals three distinct ways in which fluctuations alter the deterministic landscape. First, the effective mortality is unconditionally reduced from a to an effective parameter $a_{\mathrm{eff}} = a - s/2$, directly lowering the Allee threshold required for the front to invade the metastable state. Second, a purely noise-induced cubic term, sU^3, emerges at high densities, acting as a localized reactive push from the rear of the front. Third, the quadratic growth coefficient is weakened by a factor of $-1.5s$.

The macroscopic front velocity depends fundamentally on the stability parameter a. For small values of a, the reduction in mortality and the cubic reinforcement at the rear are anticipated to dominate. In this scenario, noise acts as a net accelerator, lifting the stochastic velocity above the deterministic benchmark. However, as a approaches unity ($a \geqslant 0.7$), the deterministic front experiences severe recession ($c_{\mathrm{det}} < 0$). In this strongly pushed regime, lowering the Allee threshold via $a_{\mathrm{eff}} = a - s/2$ reduces the recession speed, meaning that noise stabilizes the front and systematically counteracts the contraction.

Beyond the stability parameter, the renormalized framework allows us to anticipate the role of the exchange frequency μ, which controls the hyperbolic-to-diffusive transport transition. As μ increases, frequent directional reversals homogenize transport and decrease the front velocity toward the diffusive limit. Crucially, because the noise corrections are strictly reactive, they remain structurally decoupled from the hyperbolic transport mechanism. In the quasiballistic limit ($\mu \to 0$), the front profile is extremely sharp, maximizing the expression of the effective reaction terms. Conversely, as $\mu \to \infty$, diffusive spatial mixing smooths out the local nonlinear variations. We therefore predict that while all velocity curves will decay with μ, the noise-induced vertical separation will remain distinct even as μ becomes large. Because the noise corrections are confined to the reaction sector, they structurally survive the homogenization of the transport dynamics, retaining their macroscopic signature in the strongly diffusive regime.

B. Pulled regime ($a < 0$)

The pulled regime exhibits a fundamentally different algebraic structure, primarily due to the emergence of a linear term in the renormalized birth function: $b^{\mathrm{ren}}_{\mathrm{pld}}(U) = sU^3 + (1 + a - 1.5s)U^2 + (0.5s - a)U$. To understand the impact of this term, we consider the linearized growth rate at the absolute leading edge of the front, where $U \to 0$ and higher-order terms vanish. In this dilute region, the effective linear growth rate becomes $\sigma_{\mathrm{eff}} = (0.5s - a)/2$, which decomposes into the deterministic rate $\sigma_{\mathrm{det}} = -a/2$ plus a strictly positive noise contribution $s/4$. Since pulled fronts select their velocity precisely through this marginal linear stability criterion at the tip, multiplicative noise unconditionally increases the linear spreading power. Consequently, we anticipate that stochastic velocities will remain systematically higher than deterministic velocities across the entire pulled parameter space, with a sustained monotonic increase as the noise intensity s grows.

Finally, analyzing the interplay between noise and the exchange parameter μ in the pulled regime reveals a striking contrast with the pushed case. Because the velocity of pulled fronts is selected strictly by the asymptotic dynamics at the very tip ($U \to 0$), it is entirely decoupled from the nonlinear core of the front where diffusive mixing acts. The linear correction $(0.5s - a)U$ operates exactly in this asymptotic region, which remains immune to the spatial smoothing caused by frequent directional exchanges. Therefore, we predict that the acceleration induced by noise will be remarkably robust across the entire μ spectrum. Even when high exchange rates force the system into a strongly diffusive regime, the linear pull at the leading edge remains fully active, predicting that the vertical gap between stochastic and deterministic velocities will robustly survive the diffusive smoothing rather than vanishing, regardless of how large μ becomes.

These analytical deductions, derived solely from the mean-field structure of the renormalized parameters, provide a mathematically closed set of hypotheses. In the following section, we subject these predictions to high-resolution stochastic

simulations ($M = 100$) to confirm how this algebraic structure accurately dictates the macroscopic velocity selection.

III. NUMERICAL RESULTS AND DISCUSSION

We now subject the theoretical predictions formulated in Sec. II to high-resolution stochastic simulations. To isolate specific algebraic effects and guarantee numerical precision, key predictions regarding the stability parameter a and the noise intensity ε are evaluated using extended statistical ensembles ($M = 100$) equipped with 95% confidence intervals. Before discussing the physical implications of the results, we briefly detail the numerical methodology designed to capture both the hyperbolic transport and the multiplicative noise with high fidelity.

A. Numerical methodology and deterministic baseline

The deterministic and stochastic DIRW systems [Eqs. (1) and (2) and their stochastic extension] are integrated over a spatial domain $r \in [0, 400]$ discretized into $N_x = 8000$ nodes, ensuring a rigorous resolution of the sharp density gradients inherent to persistent transport. A fixed time step $\Delta t = 0.001$ is employed to maintain stability.

For the deterministic baseline, we utilize a second-order MacCormack predictor-corrector scheme. This method is particularly well suited for hyperbolic telegraph-type equations, as it accurately resolves the propagating fronts without introducing the spurious numerical diffusion that typically plagues standard Euler methods.

For the stochastic extension, it is crucial to ensure that the numerical scheme strictly respects the Stratonovich interpretation upon which our analytical renormalization is based. To achieve this, we implement a split-Heun scheme. The deterministic advection part is handled by a standard first-order upwind discretization, while the stochastic multiplicative reaction part is integrated using the Heun method (a two-stage Runge-Kutta approach). By evaluating the multiplicative noise at the predicted intermediate state, the Heun scheme naturally samples the midpoint of the stochastic integral, thereby enforcing the Stratonovich convention without requiring explicit conversion to an Itô form or the addition of external drift terms.

Regarding the effective noise parameter, ideal temporal white noise is regularized numerically by the finite time step Δt. In the continuous Stratonovich framework, the noise intensity entering the renormalized equations is defined by the integrated covariance over an infinitesimal time step, which yields unity. Consistently, in the discrete algorithm, the fluctuating parameter is implemented as $\tilde{a}_n = a + \sqrt{\varepsilon/\Delta t}\xi_n$, where ξ_n are uncorrelated standard normal variables. The discrete temporal correlation is $C_{\text{disc}}(0) = 1/\Delta t$. Consequently, the effective noise parameter that enters the continuous renormalized equations over a time step is $s = \varepsilon \times C_{\text{disc}}(0) \times \Delta t = \varepsilon$. To avoid the formal ambiguity of the continuum coincidence limit $C(0)$ associated with ideal white noise, we henceforth define the effective noise intensity directly as $s \equiv \varepsilon$, representing the finite integrated noise variance. This explicit temporal regularization ensures a mathematically consistent and finite framework for the effective field-mean theory. The front speed c is extracted via linear regression of the isodensity position

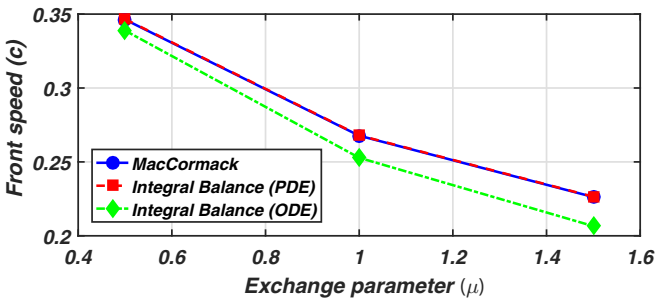


FIG. 1. Pushed regime ($a > 0$): comparison of front speeds obtained by MacCormack simulations, integral balance on PDE profiles, and integral balance on stationary ODE profiles.

$U = 0.5$ over time. Figures 1 and 2 compare MacCormack simulations against a variational integral balance (detailed in Appendix A). The excellent agreement (relative differences $<0.2\%$) validates our numerical base.

B. Direct noise intensity dependence $c(\varepsilon)$

To directly address the impact of noise intensity isolated from other parameters, we present in Fig. 3 the steady-state front velocity as a continuous function of ε for representative pushed ($a = 0.2$) and pulled ($a = -0.2$) regimes at $\mu = 1.0$. In the pulled regime, the velocity exhibits a strong, sustained monotonic increase above the deterministic benchmark ($c_{\text{det}} = 0.6255$), reaching $c = 0.7994$ at $\varepsilon = 0.5$. This clear quantitative validation confirms the analytical prediction that the linear driver $(0.5s - a)U$ dominates the leading edge dynamics, with the velocity scaling continuously with the noise intensity $s = \varepsilon$. The pushed regime displays a similar robust monotonic acceleration (from $c = 0.2774$ to $c = 0.4130$), validating the combined effect of the $a_{\text{eff}} = a - s/2$ mortality reduction and the sU^3 cubic reinforcement.

C. Stability parameter a and the macrovelocity selection

We now fix the exchange frequency to $\mu = 1.0$ to isolate the impact of the stability parameter a. Figures 4 and 5 illustrate the velocity selection for strong noise intensities across the pushed and pulled parameter spaces.

In the pushed regime (Fig. 4), the numerical results provide a clear quantitative validation of the predicted qualitative inversion. For small stability parameters ($a = 0.1$), where the deterministic speed is $c_{\text{det}} = 0.3674$, the front is systemati-

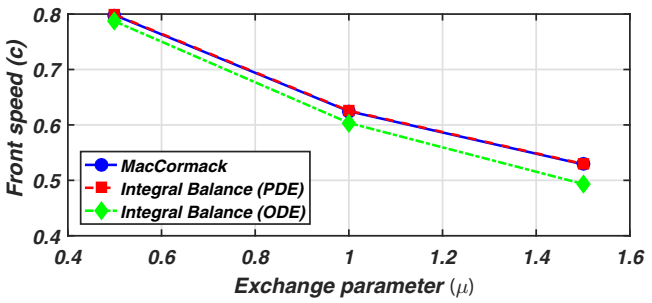


FIG. 2. Pulled regime ($a < 0$): comparison of front speeds.

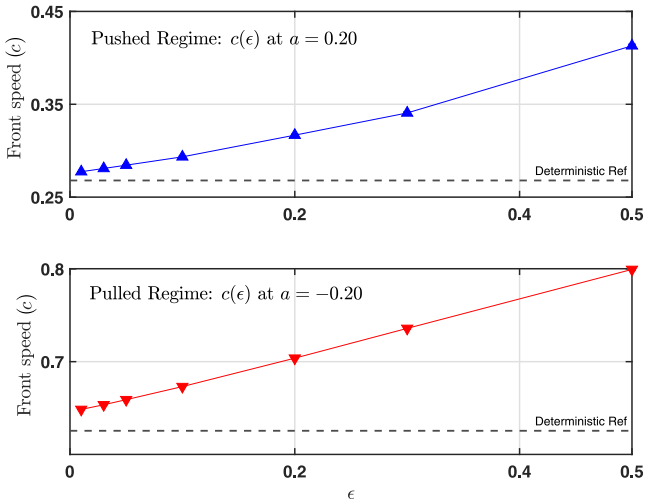


FIG. 3. Direct dependence of front velocity on noise intensity ε. Statistical 95% confidence intervals are smaller than the marker size and omitted for graphical clarity, highlighting the strong monotonic acceleration dictated by the Stratonovich drift.

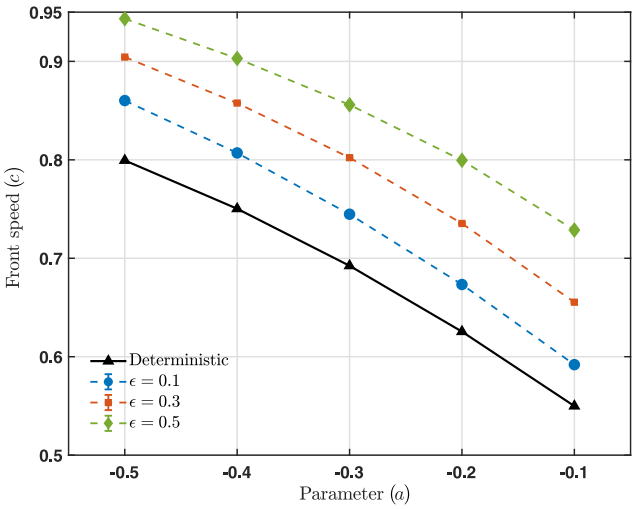


FIG. 5. Noise impact vs stability parameter a in the pulled regime ($\mu = 1.0$), highlighting the robust, sustained acceleration driven by the linearized pulling force at the leading edge.

cally accelerated by fluctuations (reaching $c_{\text{sto}} = 0.5511$ for $\varepsilon = 0.5$), driven by the mortality reduction ($a_{\text{eff}} = a - s/2$) and the cubic rear push sU^3. For intermediate stability parameters ($0.1 \leqslant a \leqslant 0.3$), the velocity curves exhibit a strong, sustained monotonic acceleration (e.g., from $c = 0.2774$ to $c = 0.4130$ at $a = 0.2$), illustrating how the noise-induced cubic term continuously reinforces the expansion. As the system transitions into a strongly pushed regime ($a \geqslant 0.7$), the deterministic front undergoes severe recession ($c_{\text{det}} < 0$) because the state $u = 0$ becomes a deep energy minimum. In this region, increasing the noise parameter s does not act as a brake to amplify the contraction, but rather dramatically reduces the recession speed (e.g., at $a = 0.9$, shifting from $c_{\text{det}} = -0.3202$ to $c_{\text{sto}} = -0.0107$ under $\varepsilon = 0.5$). By lowering the effective Allee threshold via $a_{\text{eff}} = a - s/2$, multiplicative noise counteracts the contraction and stabilizes the front against recession.

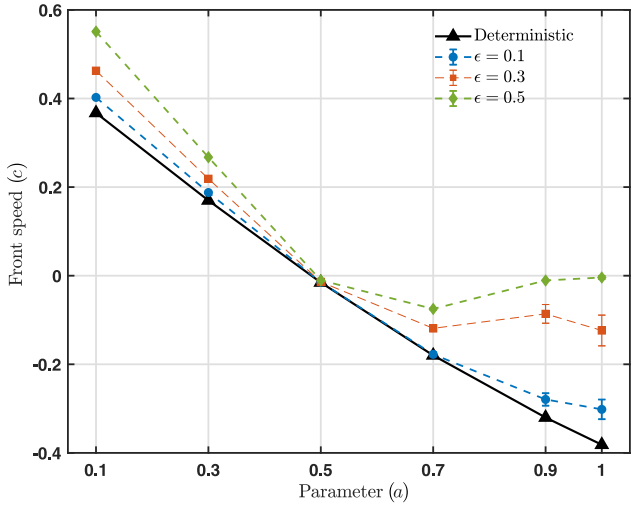


FIG. 4. Noise impact vs stability parameter a in the pushed regime ($\mu = 1.0$). The transition from acceleration to stabilization against recession is clearly visible for large a values.

In the pulled regime (Fig. 5), the unconditional nature of the noise-driven acceleration is verified across the entire parameter space. From $a = -0.5$ to $a = -0.1$, the stochastic curves remain firmly anchored above the deterministic reference, dictated by the marginal stability rate $\sigma_{\text{eff}} = (0.5s - a)/2$ at the leading edge. For instance, at $a = -0.2$, the velocity increases strongly from $c_{\text{det}} = 0.6255$ to $c_{\text{sto}} = 0.7995$ at $\varepsilon = 0.5$. This sustained monotonic increase confirms that the nonlinear field-mean framework accurately captures the dominant role of the Stratonovich-induced linear growth term.

Together, these numerical results demonstrate that the renormalized field-mean framework does more than predict qualitative trends; it precisely accounts for the macroscopic velocity selection, offering a closed, quantitatively accurate description of noise-constrained persistent random walks. A distinctive structural feature of this persistent walk model is the decoupling between the purely reactive noise corrections and the hyperbolic transport operator. While standard parabolic reaction-diffusion systems also exhibit noise-induced velocity shifts, their coupled diffusive spatial dynamics intertwine reaction and transport, complicating the isolation of purely reactive noise signatures. In contrast, the DIRW framework allows the multiplicative noise signature to be algebraically isolated within the reaction sector. This structural decoupling explains why the noise-induced velocity shift remains robust even as the exchange rate μ increases and the transport sector transitions toward a diffusive regime.

IV. CONCLUSION

In this work, we have established a comprehensive and quantitatively precise account of noise-constrained velocity selection in persistent reaction random walks. By applying nonperturbative renormalization theory to the DIRW framework, we derived effective reaction terms that revealed a rich, hidden algebraic structure governing front propagation

under multiplicative fluctuations. High-resolution stochastic PDE simulations using extended statistical ensembles ($M = 100$) and a rigorously implemented split-Heun scheme for Stratonovich calculus have successfully validated these theoretical predictions.

Our primary finding is that the impact of multiplicative noise depends sensitively on the underlying stability landscape and the specific algebraic terms involved, rather than acting as a universal suppressor. In pushed fronts, noise reveals a dual entity: it acts as an accelerator driven by reduced effective mortality ($a_{\text{eff}} = a - s/2$) and cubic reinforcement at small stability parameters (a), but acts as a critical stabilizing mechanism against front recession at large a values by counteracting severe contractions. In pulled fronts, the emergence of the linear driver rate at the leading edge ensures a strong, sustained monotonic acceleration as noise intensity increases.

By establishing the direct noise intensity dependence $c(\varepsilon)$ alongside rigorous numerical diagnostics, this study delivers a robust, falsifiable framework for stochastic front dynamics. It isolates the purely reactive nature of multiplicative fluctuations within the DIRW framework, highlighting how the strict structural decoupling between reaction and transport allows these noise signatures to persist across the hyperbolic-to-diffusive transition. This work sets the stage for broader applications in biological invasion fronts, chemical kinetics, and active matter systems, where directional persistence and stochasticity are intrinsic, intertwined fundamental mathematical and physical features of transport.

DATA AVAILABILITY

The numerical data that support the findings of this study, including the ensemble averages (M=100) and the 95% confidence intervals used to generate the figures, are available from the corresponding author upon reasonable request.

APPENDIX A: VARIATIONAL DETERMINATION OF THE WAVE SPEED

We present a variational method for determining the propagation speed c of traveling wave solutions in the DIRW system. The approach proceeds through a systematic sequence of algebraic manipulations and integrations, culminating in a closed expression for c.

1. Step 1: Corrected system

In the traveling wave frame, the system is written as

$$(\gamma - c)U^{+'} = \mu(U^- - U^+) + \tfrac{1}{2}b(U) - d(U)U^+, \quad \text{(A1)}$$

$$(\gamma + c)U^{-'} = -\mu(U^+ - U^-) - \tfrac{1}{2}b(U) + d(U)U^-. \quad \text{(A2)}$$

2. Step 2: Multiplication by derivatives

Each equation is multiplied by the derivative of its respective variable:

$$(\gamma - c)(U^{+'})^2 = \left[\mu(U^- - U^+) + \tfrac{1}{2}b(U) - d(U)U^+\right]U^{+'}, \quad \text{(A3)}$$

$$(\gamma + c)(U^{-'})^2 = \left[-\mu(U^+ - U^-) - \tfrac{1}{2}b(U) + d(U)U^-\right]U^{-'}. \quad \text{(A4)}$$

3. Step 3: Summation and subtraction before integration

Rather than integrating each equation individually, we first combine them. The sum and difference yield

$$\begin{aligned}(\gamma - c)(U^{+'})^2 + (\gamma + c)(U^{-'})^2 &= \left[\mu(U^- - U^+) + \tfrac{1}{2}b(U) - d(U)U^+\right]U^{+'} \\ &\quad + \left[-\mu(U^+ - U^-) - \tfrac{1}{2}b(U) + d(U)U^-\right]U^{-'}, \quad \text{(A5)}\end{aligned}$$

$$\begin{aligned}(\gamma - c)(U^{+'})^2 - (\gamma + c)(U^{-'})^2 &= \left[\mu(U^- - U^+) + \tfrac{1}{2}b(U) - d(U)U^+\right]U^{+'} \\ &\quad - \left[-\mu(U^+ - U^-) - \tfrac{1}{2}b(U) + d(U)U^-\right]U^{-'}. \quad \text{(A6)}\end{aligned}$$

Combining before integration allows for a more favorable cancellation structure when integrating over the domain.

4. Step 4: Integration

Integrating over $\mathbb{R}$ gives

$$\begin{aligned}(\gamma - c)\int_{-\infty}^{+\infty}(U^{+'})^2\,dz + (\gamma + c)\int_{-\infty}^{+\infty}(U^{-'})^2\,dz &= \int_{-\infty}^{+\infty}\left[\mu(U^- - U^+) + \frac{1}{2}b(U) - d(U)U^+\right]U^{+'}\,dz \\ &\quad + \int_{-\infty}^{+\infty}\left[-\mu(U^+ - U^-) - \frac{1}{2}b(U) + d(U)U^-\right]U^{-'}\,dz, \quad \text{(A7)}\end{aligned}$$

$$\begin{aligned}(\gamma - c)\int_{-\infty}^{+\infty}(U^{+'})^2\,dz - (\gamma + c)\int_{-\infty}^{+\infty}(U^{-'})^2\,dz &= \int_{-\infty}^{+\infty}\left[\mu(U^- - U^+) + \frac{1}{2}b(U) - d(U)U^+\right]U^{+'}\,dz \\ &\quad - \int_{-\infty}^{+\infty}\left[-\mu(U^+ - U^-) - \frac{1}{2}b(U) + d(U)U^-\right]U^{-'}\,dz. \quad \text{(A8)}\end{aligned}$$

5. Step 5: Elimination of B

By adding and subtracting the two integrated relations, the terms involving $B = \int (U^{-'})^2\,dz$ cancel. This leaves a relation expressed solely in terms of

$$A = \int_{-\infty}^{+\infty}(U^{+'})^2\,dz, \quad \text{(A9)}$$

along with the associated reaction-transport integrals. The denominator thus reduces to A alone.

6. Step 6: Final velocity formula

The resulting expression for the wave speed is

$$\boxed{c = \gamma - \frac{I_+}{A}}, \quad \text{(A10)}$$

where the numerator integral is defined as

$$I_+ = \int_{-\infty}^{+\infty}\left[\mu(U^- - U^+) + \frac{1}{2}b(U) - d(U)U^+\right]U^{+'}\,dz. \quad \text{(A11)}$$

This formulation provides a robust and physically transparent means of evaluating the wave speed directly from the computed wave profiles, with the denominator relying only on the gradient norm of the U^+ component.

APPENDIX B: RENORMALIZED REACTION TERMS DERIVATION

We detail here the step-by-step derivation of the renormalized birth and death terms, $b^{\text{ren}}(U)$ and $d^{\text{ren}}(U)$, using a nonperturbative framework based on the Furutsu-Novikov-Donsker (FND) theorem for multiplicative noise [21,26].

General FND framework. The stochastic extension of the DIRW system for the right-moving density u^+ is governed by

$$\frac{\partial u^+}{\partial t} = \cdots + R^+(u, u^+, a) + \varepsilon^{1/2} g_1(u^+, u^-)\xi(t), \tag{B1}$$

where $R^+(u, u^+, a) = \frac{1}{2}b(u) - d(u)u^+$ represents the deterministic reaction kinetics. The multiplicative noise coupling function g_1 is rigorously defined as the parametric sensitivity of the reaction sector with respect to the fluctuating control parameter a:

$$g_1(u^+, u^-) = \frac{\partial R^+}{\partial a}. \tag{B2}$$

To evaluate the statistical ensemble average of the multiplicative term $\langle g_1(u^+, u^-)\xi(t)\rangle$, the FND theorem stipulates that for a Gaussian process $\xi(t)$ with a correlation function $C(t - t')$, the average can be expressed via functional differentiation:

$$\langle g_1(u^+, u^-)\xi(t)\rangle = \int_0^t C(t - t')\left\langle \frac{\delta g_1(u^+(t), u^-(t))}{\delta \xi(t')} \right\rangle dt'. \tag{B3}$$

Applying the functional chain rule maps the sensitivity of the coupling function onto the causal response functions (Green's functions) of the hyperbolic transport fields:

$$\frac{\delta g_1(u^+(t), u^-(t))}{\delta \xi(t')} = \frac{\partial g_1}{\partial u^+}\frac{\delta u^+(t)}{\delta \xi(t')} + \frac{\partial g_1}{\partial u^-}\frac{\delta u^-(t)}{\delta \xi(t')}. \tag{B4}$$

In the short-memory limit imposed by the Stratonovich interpretation, the temporal correlation $C(t - t')$ acts strictly at $t' \to t^-$. For multivariate systems subjected to a purely temporal global noise $\xi(t)$, the nonanticipating functional derivative evaluation in the Stratonovich convention prescribes that the correlation is entirely captured by the local algebraic coupling of the state variables. Consequently, the FND integral reduces directly to the trace of the product of the sensitivity functions and their state derivatives, yielding the exact systematic Stratonovich correction (incorporating the standard $1/2$ factor of the Stratonovich convention):

$$\Delta R^+ = \frac{1}{2}s\left(g_1\frac{\partial g_1}{\partial u^+} + g_2\frac{\partial g_1}{\partial u^-}\right), \tag{B5}$$

where $s \equiv \varepsilon$ denotes the finite integrated noise intensity (avoiding the ill-defined pointwise coincidence limit of white noise), and $g_2 = \partial R^-/\partial a$. The effective mean-field description for the macrodynamics thus becomes $\langle \partial_t u^+\rangle = \cdots + R^+ + \Delta R^+$.

It is instructive to consider how alternative stochastic interpretations would affect this renormalization procedure. Under the Itô convention, the functional derivative evaluation obeys a strictly nonanticipative causality requirement, meaning that the system density cannot respond instantaneously to an ongoing noise pulse. Mathematically, this enforces the property $\lim_{t' \to t^-} \delta u^{\pm}(t)/\delta \xi(t') = 0$ since the stochastic integrals are evaluated at the left endpoint of each temporal subinterval. Consequently, the FND integral vanishes identically, leading to a zero noise correction ($\Delta R^+ = 0$). Under an Itô framework, the deterministic macroscopic kinetics are preserved without structural drift, meaning that the noise-induced transitions between pushed and pulled front regimes, as well as the renormalization of the birth and death bounds described in Sec. III, are intrinsically unique to the Stratonovich interpretation of the multiplicative environmental noise.

1. Pushed regime ($a > 0$)

Step 1. Deterministic reaction term:

$$R^+_{\text{psd}} = \tfrac{1}{2}(1 + a)u^2 - (u^2 + a)u^+. \tag{B6}$$

Step 2. Differentiating with respect to a:

$$g_1^{\text{psd}} = \tfrac{1}{2}u^2 - u^+, \quad g_2^{\text{psd}} = \tfrac{1}{2}u^2 - u^-. \tag{B7}$$

Partial derivatives with respect to the density components:

$$\frac{\partial g_1^{\text{psd}}}{\partial u^+} = u - 1, \quad \frac{\partial g_1^{\text{psd}}}{\partial u^-} = u. \tag{B8}$$

Step 3. Noise correction evaluation:

$$\begin{aligned}\Delta R^+_{\text{psd}} &= \tfrac{1}{2}s\left[\left(\tfrac{1}{2}u^2 - u^+\right)(u - 1) + \left(\tfrac{1}{2}u^2 - u^-\right)u\right] \\ &= \tfrac{1}{2}s\left[u^3 - \tfrac{3}{2}u^2 - u(u^+ + u^-) + u^+\right] \\ &= \tfrac{1}{2}s\left(u^3 - \tfrac{3}{2}u^2 + u^+\right).\end{aligned} \tag{B9}$$

Step 4. Assembling the mean field:

$$\begin{aligned}\langle \partial_t u^+\rangle &= \cdots + \left[\tfrac{1}{2}(1 + a)u^2 - (u^2 + a)u^+\right] \\ &\quad + \tfrac{1}{2}s\left(u^3 - \tfrac{3}{2}u^2 + u^+\right) \\ &= \tfrac{1}{2}[(1 + a - 1.5s)u^2 + su^3] - (u^2 + a - 0.5s)u^+.\end{aligned} \tag{B10}$$

By defining U as the macroscopic mean field, this identifies the renormalized forms:

$$\begin{aligned}b^{\text{ren}}_{\text{psd}}(U) &= sU^3 + (1 + a - 1.5s)U^2, \\ d^{\text{ren}}_{\text{psd}}(U) &= U^2 + a - 0.5s.\end{aligned} \tag{B11}$$

2. Pulled regime ($a < 0$)

Step 1. Deterministic reaction term:

$$R^+_{\text{pld}} = \tfrac{1}{2}((1 + a)u^2 - au) - u^2u^+. \tag{B12}$$

Step 2. Differentiating with respect to a:

$$g_1^{\text{pld}} = \tfrac{1}{2}(u^2 - u), \quad g_2^{\text{pld}} = \tfrac{1}{2}(u^2 - u). \tag{B13}$$

Partial derivatives with respect to the density components:

$$\frac{\partial g_1^{\text{pld}}}{\partial u^+} = \frac{\partial g_1^{\text{pld}}}{\partial u^-} = u - \frac{1}{2}. \tag{B14}$$

Step 3. Noise correction evaluation:

$$\begin{aligned}\Delta R^+_{\text{pld}} &= \frac{1}{2}s\left[g_1^{\text{pld}}\frac{\partial g_1^{\text{pld}}}{\partial u^+} + g_2^{\text{pld}}\frac{\partial g_1^{\text{pld}}}{\partial u^-}\right] \\ &= s\left[\frac{1}{2}(u^2-u)\left(u-\frac{1}{2}\right)\right] \\ &= \frac{1}{2}s\left(u^3 - \frac{3}{2}u^2 + \frac{1}{2}u\right).\end{aligned} \tag{B15}$$

Step 4. Assembling the mean field:

$$\begin{aligned}\langle \partial_t u^+\rangle &= \cdots + \left[\tfrac{1}{2}(1+a)u^2 - \tfrac{1}{2}au - u^2u^+\right] \\ &\quad + \tfrac{1}{2}s\left(u^3 - \tfrac{3}{2}u^2 + \tfrac{1}{2}u\right) \\ &= \tfrac{1}{2}[(1+a-1.5s)u^2 + su^3 + (0.5s-a)u] - (u^2)u^+.\end{aligned} \tag{B16}$$

Expressing the result in terms of the macroscopic profile U yields:

$$\begin{aligned}b^{\text{ren}}_{\text{pld}}(U) &= sU^3 + (1+a-1.5s)U^2 + (0.5s-a)U, \\ d^{\text{ren}}_{\text{pld}}(U) &= U^2.\end{aligned} \tag{B17}$$

This confirms the emergence of the crucial linear correction $(0.5s-a)U$ in $b^{\text{ren}}_{\text{pld}}(U)$, driving the pulled front dynamics discussed in Sec. III.

[1] R. A. Fisher, The wave of advance of advantageous genes, Ann. Eug. **7**, 355 (1937).

[2] J. D. Murray, *Mathematical Biology* (Springer, New York, 2002).

[3] M. C. Cross and P. C. Hohenberg, Pattern formation outside of equilibrium, Rev. Mod. Phys. **65**, 851 (1993).

[4] J. Keener and J. Sneyd, *Mathematical Physiology* (Springer, New York, 1998).

[5] T. Jonckheere, C. A. Müller, R. Kaiser, C. Miniatura, and D. Delande, Multiple scattering of light by atoms in the weak localization regime, Phys. Rev. Lett. **85**, 4269 (2000).

[6] J. Nagumo, S. Arimoto, and S. Yoshizawa, An active pulse transmission line simulating nerve axon, Proc. IRE **50**, 2061 (1962).

[7] A. Kolmogorov, I. Petrovskii, and N. Piskunov, A study of the diffusion equation with increase in the amount of substance, and its application to a biological problem, Bull. Moscow Univ. Math. Mech. **1**, 1 (1937).

[8] W. Horsthemke, Spatial instabilities in reaction random walks with direction-independent kinetics, Phys. Rev. E **60**, 2651 (1999).

[9] G. H. Weiss, *Aspects and Applications of the Random Walk* (North-Holland, Amsterdam, 1994).

[10] R. Sambeth and A. Baumgaertner, Autocatalytic polymerization generates persistent random walk of crawling cells, Phys. Rev. Lett. **86**, 5196 (2001).

[11] S. Huang, C. P. Brangwynne, K. K. Parker, and D. E. Ingber, Symmetry-breaking in mammalian cell cohort migration during tissue pattern formation: Role of random-walk persistence, Cell Motil. Cytosk. **61**, 201 (2005).

[12] Z. Sadjadi, M. Reza Shaebani, H. Rieger, and L. Santen, Persistent-random-walk approach to anomalous transport of self-propelled particles, Phys. Rev. E **91**, 062715 (2015).

[13] J. Kent-Dobias, Very persistent random walkers reveal transitions in landscape topology, Phys. Rev. Lett. **136**, 117401 (2026).

[14] H. G. Othmer and A. Stevens, Aggregation, blowup, and collapse: The ABC's of taxis in reinforced random walks, SIAM J. Appl. Math. **57**, 1044 (1997).

[15] K. E. Hyland, S. McKee, and M. W. Reeks, Derivation of a pdf kinetic equation for the transport of particles in turbulent flows, J. Phys. A: Math. Gen. **32**, 6169 (1999).

[16] M. E. Cates and J. Tailleur, When are active Brownian particles and run-and-tumble particles equivalent? Consequences for motility-induced phase separation, Europhys. Lett. **101**, 20010 (2013).

[17] N. Razin, Entropy production of an active particle in a box, Phys. Rev. E **102**, 030103(R) (2020).

[18] D. Frydel, Generalized run-and-tumble model in 1D geometry for an arbitrary distribution of drift velocities, J. Stat. Mech. (2021) 083220.

[19] W. van Saarloos, Front propagation into unstable states, Phys. Rep. **386**, 29 (2003).

[20] E. Brunet and B. Derrida, Shift in the velocity of a front due to a cutoff, Phys. Rev. E **56**, 2597 (1997).

[21] J. Armero, J. Casademunt, L. Ramírez-Piscina, and J. M. Sancho, Ballistic and diffusive corrections to front propagation in the presence of multiplicative noise, Phys. Rev. E **58**, 5494 (1998).

[22] D. Panja, Effects of fluctuations on propagating fronts, Phys. Rep. **393**, 87 (2004).

[23] K. Furutsu, On the statistical theory of electromagnetic waves in a fluctuating medium (I), J. Res. Natl. Bur. Stand. Sect. D **67**, 303 (1963).

[24] E. A. Novikov, Functionals and the random-force method in turbulence theory, Sov. Phys. JETP **20**, 1290 (1965).

[25] M. Donsker and S. Varadhan, *Analysis of Functionals* (Springer, Berlin, 1979).

[26] J. García-Ojalvo and J. M. Sancho, *Noise in Spatially Extended Systems* (Springer, New York, 1999).